Supplement of The Cryosphere, 19, 375–392, 2025
https://doi.org/10.5194/tc-19-375-2025-supplement

The Cryosphere Open Access EGU

Supplement of

Evidence of active subglacial lakes under a slowly moving coastal region of the Antarctic Ice Sheet

Jennifer F. Arthur et al.

Correspondence to: Jennifer F. Arthur (jennifer.arthur@npolar.no)

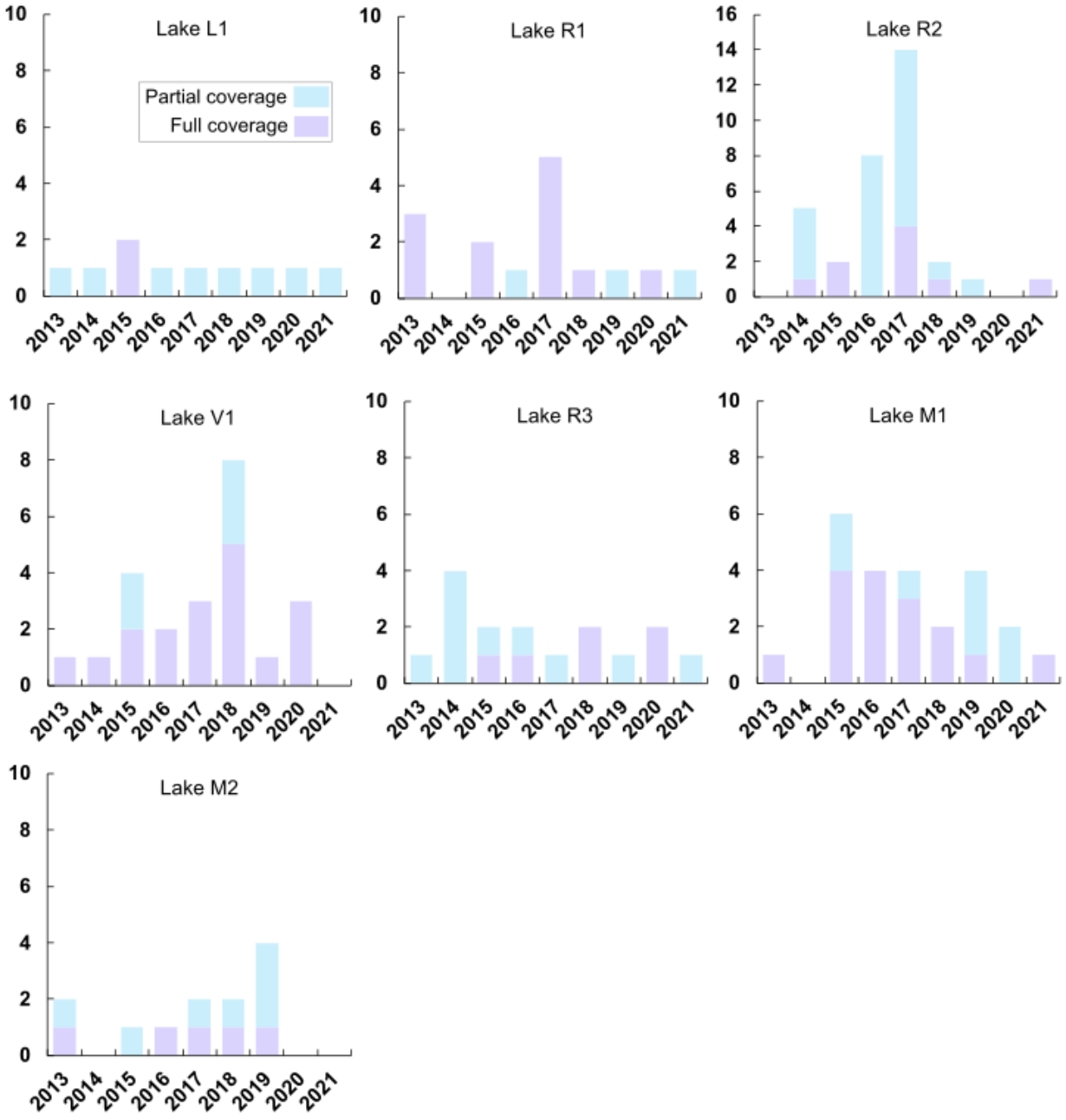

Fig. S1: Availability of time-stamped 2-m REMA strips over lakes identified from satellite altimetry, coloured according to partial coverage (blue) or full coverage (purple) of each lake.

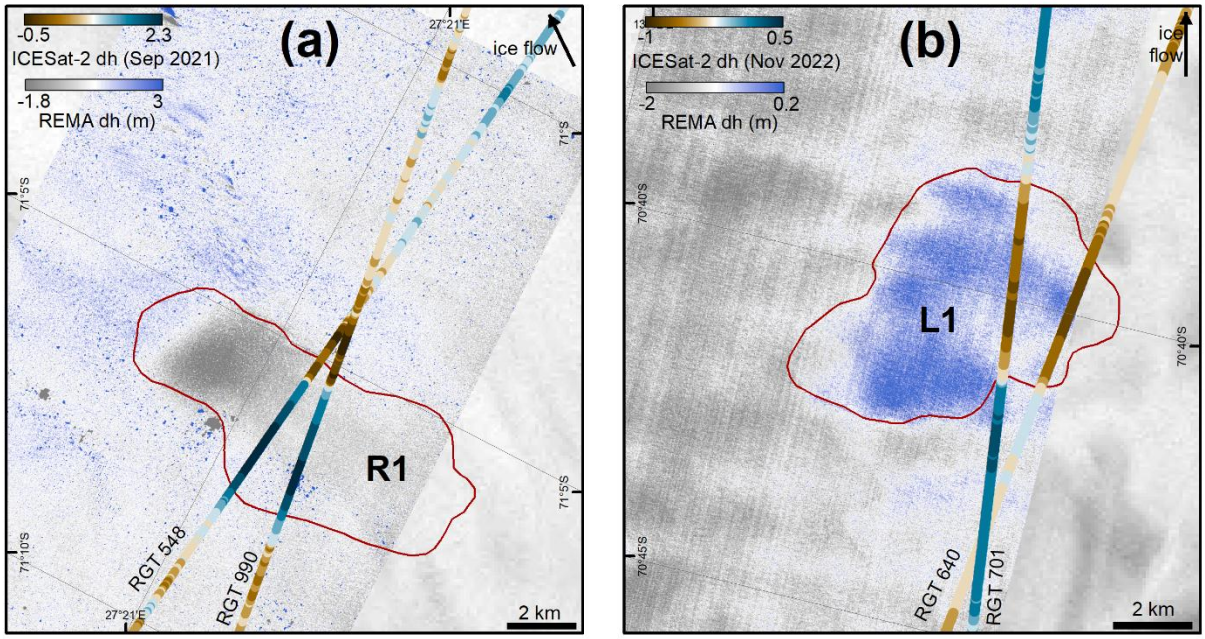

Fig. S2: Ice surface elevation change from REMA strip differencing for Lakes R1 (a) and L1 (b). Regions of ice surface subsidence (yellow shading) between time-stamped REMA strip pairs (7th December 2016 – 21st December 2017 and 12th September 2015 – 10th December 2016) are delineated by the dashed lines. Each example highlights the spatial cooccurrence between localised ice surface subsidence and surface elevation anomalies along the intersecting ICESat-2 tracks, suggesting Lakes R1 and L1 were draining during the period bounded by the REMA strip pairs.

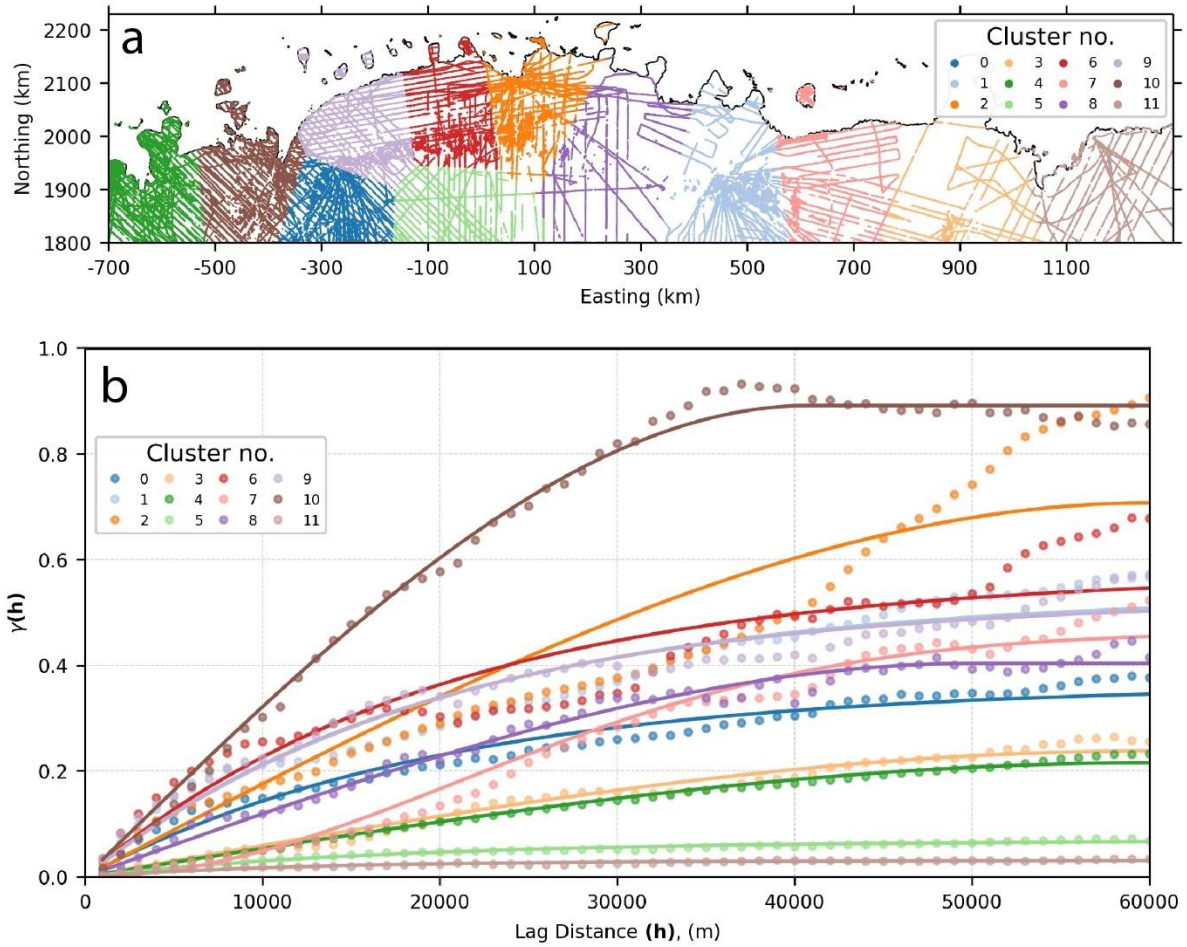

Fig. S3: Clustered bed elevation data and associated variograms. a) Map showing radar-survey derived bed elevation data divided into 12 regional clusters using a k-means clustering algorithm on measurement coordinates. Map is in a polar stereographic projection with true scale latitude of -71 and central longitude of 10 degrees. b) Experimental variogram (points) and modelled variogram (curves) are shown for normalised bed elevations in each of the 12 regions. The best-fitting model types are either exponential (clusters 0,5,6,9,11), spherical (clusters 1,2,3,4,8,10) or Gaussian (cluster 7).

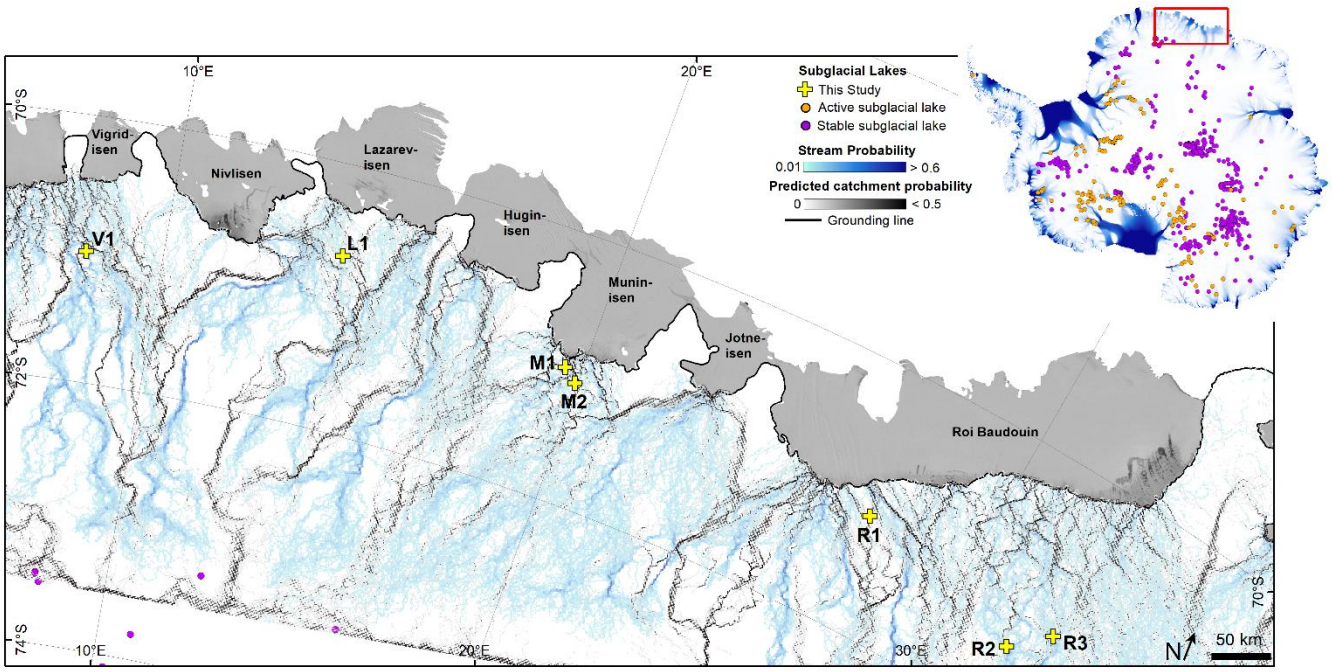

Fig. S4: Probability of subglacial drainage catchment boundaries derived from water routing analyses over the ensemble of 50 stochastic bed simulations. The dashed black line is the MEaSUREs grounding line (Rignot et al., 2016) and ice-shelf imagery is from the MODIS mosaic (Haran et al., 2021). Subglacial lake locations depicted in the inset map are from Livingstone et al. (2022), where active lakes are represented by orange dots and stable lakes by green dots. Simulations of subglacial water drainage pathways are limited to ca. <73°.

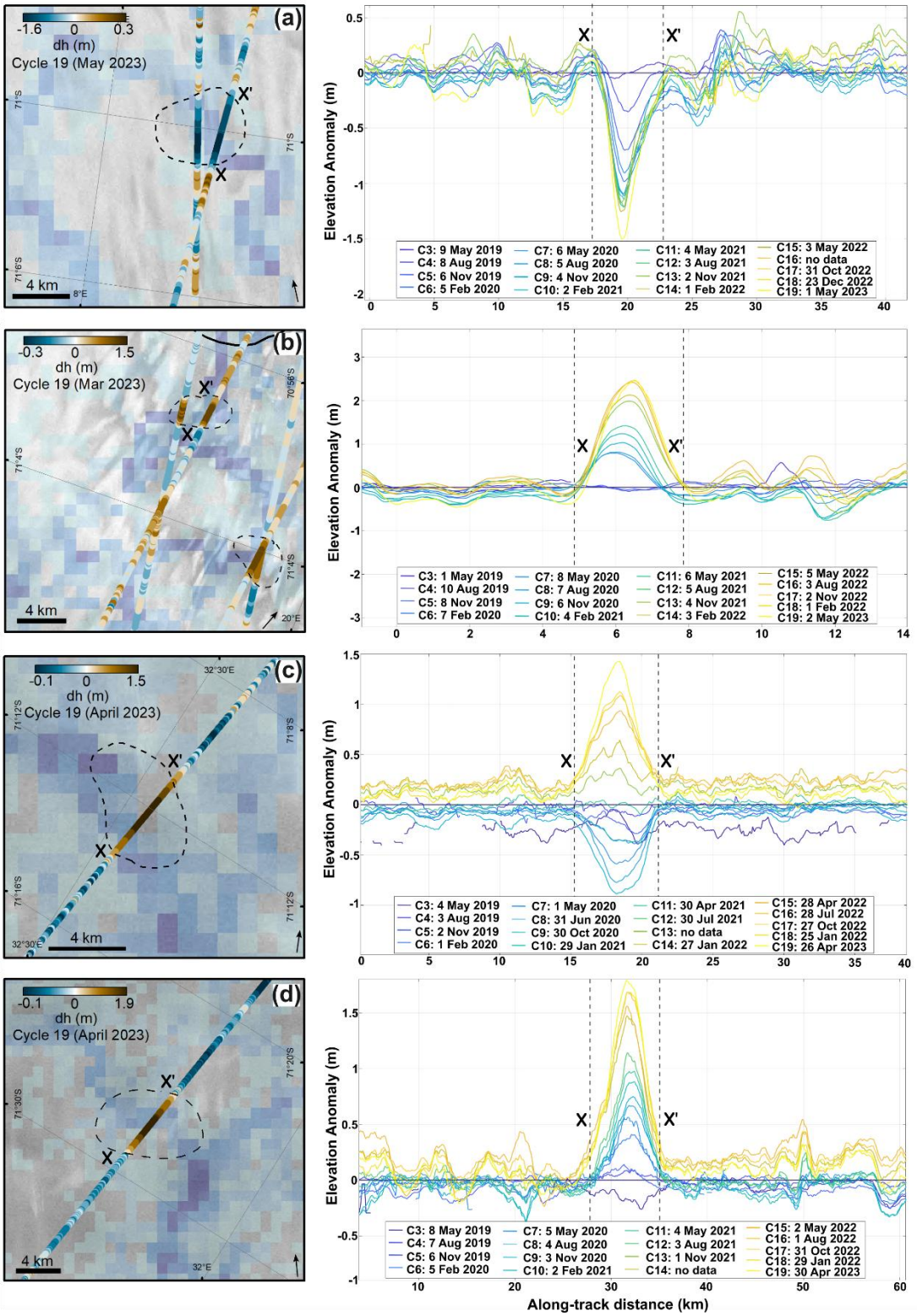

Fig. S5: Ice surface elevation displacements for Lakes V1, M1, M2, R2 and R3 derived from ICESat-2. Transects X-X' in each panel highlight significant (>1 m) ice surface elevation anomalies along ICESat-2 tracks. Graphs show along-track ice surface elevation displacements relative to ICESat-2 Cycle 3 (April/May 2019). Colours correspond to individual ICESat-2 cycles.

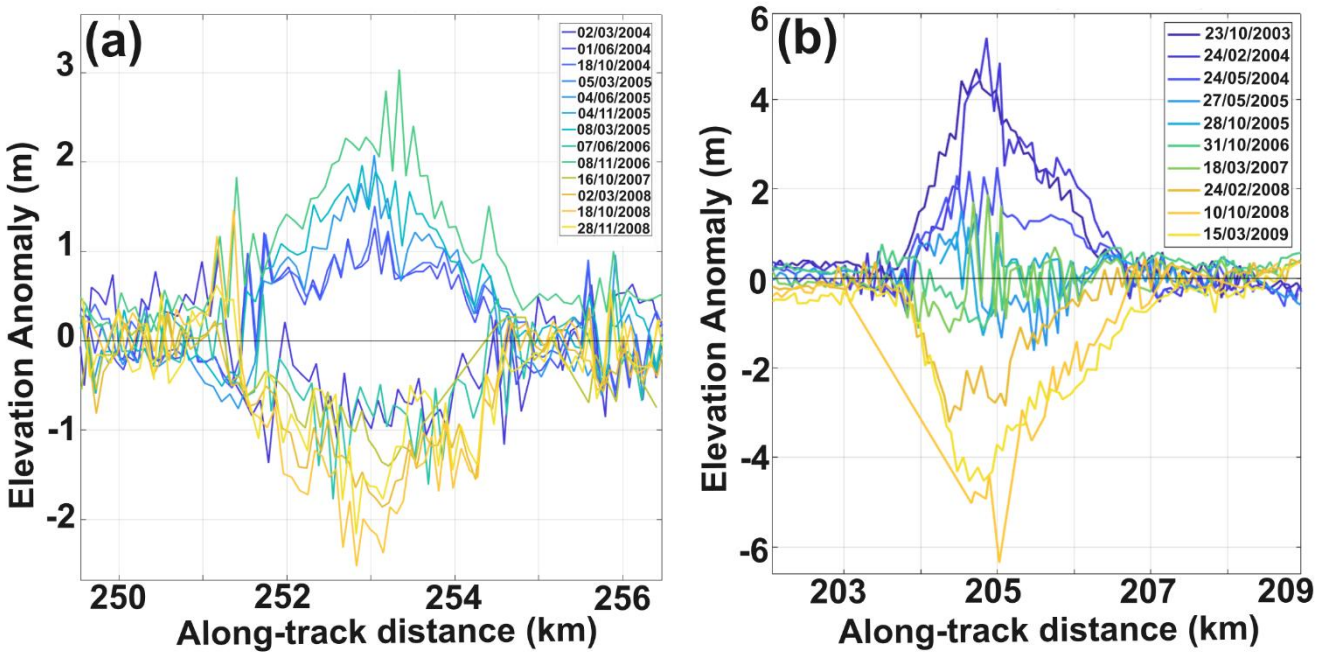

Fig. S6: Ice surface elevation displacement anomalies from two ICESat tracks over Lake R1 (a, Track 21) and Lake L1 (b, Track 134). Elevation anomalies are calculated with respect to surface plane fits representing averaged surface elevation.

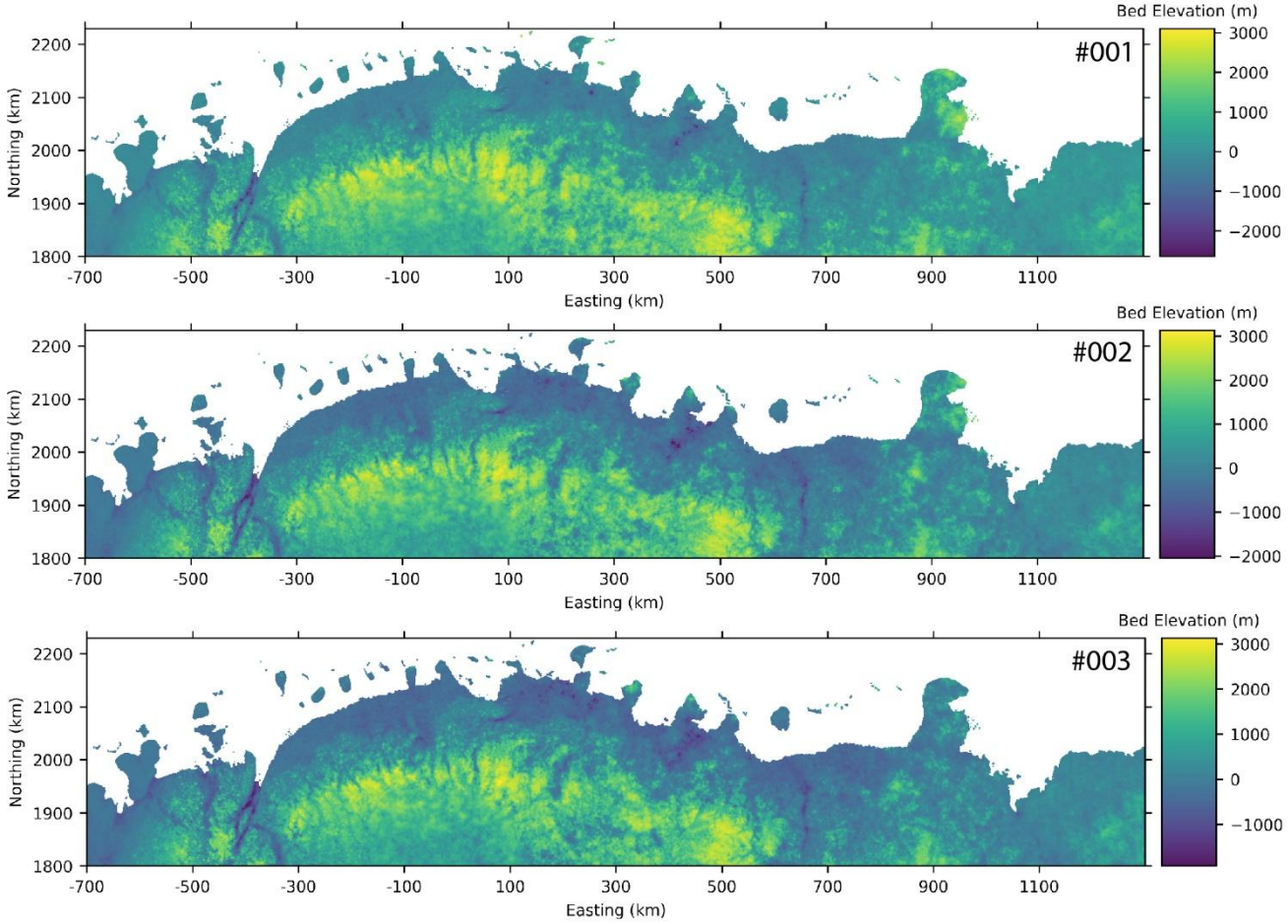

Fig. S7: Example of simulated bed elevation results 001-003 out of the ensemble of 50 equally-likely grids. Map is in a polar stereographic projection with true scale latitude of -71 and central longitude of 10 degrees.

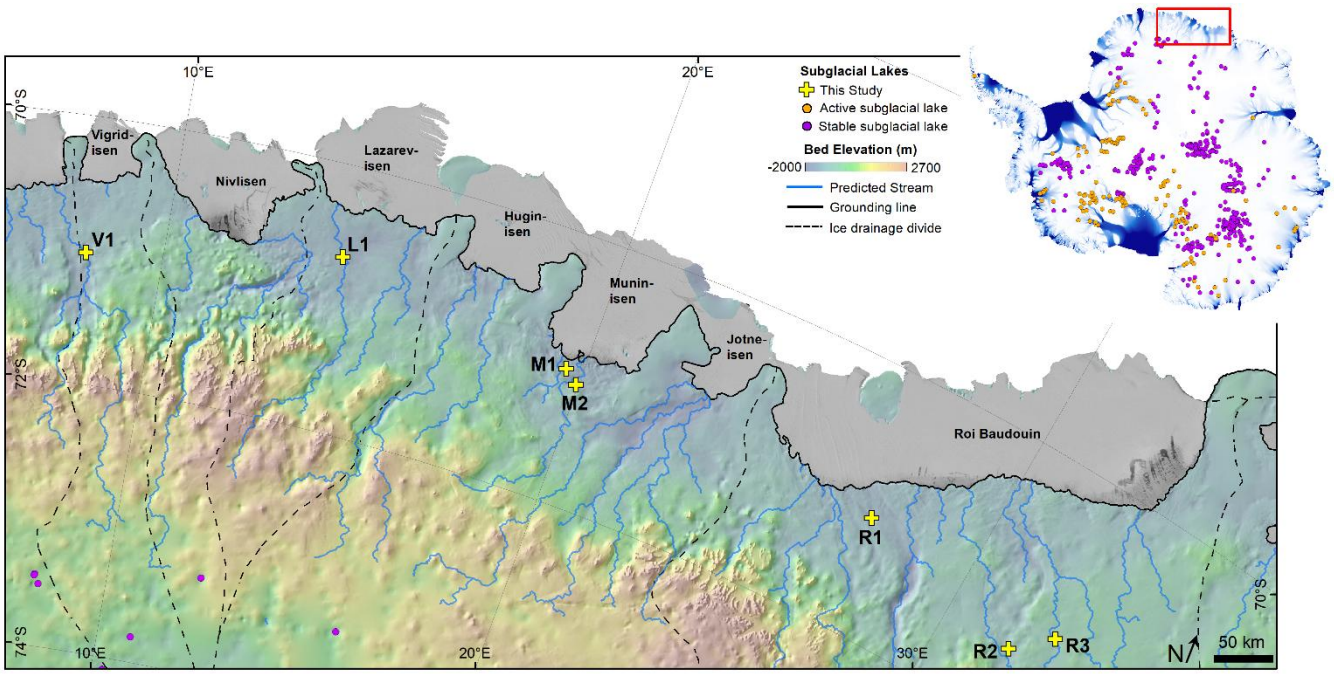

Fig. S8: Example of predicted streams from water routing analysis for one of 50 stochastic simulations. Newly-identified active lakes in this study are shown in yellow and previously identified subglacial lakes from Goeller et al. (2016) are shown in purple. The dashed black line is the MEaSUREs grounding line (Rignot et al., 2016) and the bed elevations are from BedMachine (Morlighem et al., 2022). Ice-shelf imagery is from the MODIS mosaic (Haran et al., 2021). Subglacial lake locations depicted in the inset map are from Livingstone et al. (2022), where active lakes are represented by orange dots and stable lakes by green dots. Simulations of subglacial water drainage pathways are limited to ca. <73°.

Table S1: Details of time-stamped 2-m REMA strips used for DEM differencing, including vertical elevation bias from co-registration with ICESat-2 (calculated as the average difference between DEM strip elevations and closest contemporaneous ICESat-2 elevations along overlapping ICESat-2 tracks), standard deviation in elevation bias and time difference between REMA strip acquisition date and the closest contemporaneous ICESat-2 elevation data. Elevation bias and time difference could not be calculated for the four last strips due to lacking contemporaneous ICESat-2 data.

REMA Strip Date	Location	Satellite	Elevation bias from ICESat-2 (m)	σ (m)	Time difference (days)
22nd October 2019	Roi Baudouin Ice Shelf	Worldview-1	-0.70	0.52	69
10th January 2021	Roi Baudouin Ice Shelf	Worldview-2	-2.41	1.20	15
18th January 2021	Roi Baudouin Ice Shelf	Worldview-1	-0.98	0.29	11
28th December 2022	Roi Baudouin Ice Shelf	Worldview-1	0.52	0.24	62
25th January 2020	Lazarev Ice Shelf	Worldview-1	3.53	0.42	12
15th February 2021	Lazarev Ice Shelf	Worldview-3	-2.10	0.42	12
12th September 2015	Lazarev Ice Shelf	Worldview-1	-		-
10th December 2016	Lazarev Ice Shelf	Worldview-1	-		-
7th December 2016	Roi Baudouin Ice Shelf	Worldview-1	-		-
21st December 2017	Roi Baudouin Ice Shelf	Worldview-1	-		-